International Journal of Solids and Structures 58 (2015) 301–308

Contents lists available at ScienceDirect

International Journal of Solids and Structures

journal homepage: www.elsevier.com/locate/ijsolstr

Dynamic stability of a bar under high loading rate: Response to local perturbations

K. Ravi-Chandar [b,a], N. Triantafyllidis [a,c,d,*]

[a] Laboratoire de Mécanique des Solides, C.N.R.S. UMR7649, École Polytechnique, Palaiseau 91128, France
[b] Aerospace Engineering & Engineering Mechanics Department, The University of Texas, Austin, TX 78712-0235, USA
[c] Département de Mécanique, École Polytechnique, Palaiseau 91128, France
[d] Aerospace Engineering Department & Mechanical Engineering Department (emeritus), The University of Michigan, Ann Arbor, MI 48109-2140, USA

ARTICLE INFO

Article history:
Received 23 May 2014
Received in revised form 19 August 2014
Available online 20 October 2014

Keywords:
Inertia
Energy methods
Nonlinear elasticity

ABSTRACT

Of interest here is the influence of loading rate on the stability of structures where inertia is taken into account. The approach currently used in the literature to analyze these stability problems, is the method of modal analysis that determines the structure's fastest growing wavelength, which is meaningful only for cases where the velocity of the perfect structure is significantly lower than the associated characteristic wave propagation speeds. The novel idea here is to analyze the time-dependent response to perturbations of the transient (high strain rates) states of these structures, in order to understand the initiation of the corresponding failure mechanisms.

We are motivated by the recent experimental studies of Zhang and Ravi-Chandar (2006) on the high strain rate extension of thin rings that show no evidence of a dominant wavelength in their failure mode and no influence of strain-rate sensitivity on the necking strains. In the interest of analytical tractability, we study the extension of an incompressible, nonlinearly elastic bar at different strain rates. The dynamic stability of these bars is studied by following the evolution of localized small perturbations introduced at different times. It is shown that these structures are stable until the static necking strain is reached at some point. Moreover their failure pattern is dictated by the distribution of defects, the minimum distance between necks diminishes with increasing strain rate and there is no dominant wavelength mode, exactly as observed experimentally in Zhang and Ravi-Chandar (2006).

1. Introduction

The issue of dynamic stability of structures is an important engineering problem and as such has drawn considerable attention. The first investigation in this area appears to be the work of Koning and Taub (1933), who investigated the influence of inertia in a simply supported imperfect column subjected to a sudden axial load. A substantial amount of work followed that investigated the response of, mainly elastic, structures to impulse or time-dependent loads. As a result, and due to the many possible definitions for the stability of time-dependent systems, the term *dynamic stability* encompasses many classes of problems and different physical phenomena and has many interpretations, with inertia being the only common denominator.

In the absence of inertia, the processes of failure by a bifurcation instability mode in elastic solids and structures is well understood (e.g. Brush and Almroth, 1975) and a general asymptotic analysis, termed Lyapunov–Schmidt–Koiter (LSK), has been developed for their study. The first effort to use the LSK general analysis for the dynamic stability problem of an elastic structure appears to be Budiansky and Hutchinson (1964), where the authors proposed an asymptotic analysis of the time-dependent problem using the eigenmodes of the static problem.

Another idea, popular in fluid mechanics, has also been adopted for the dynamic stability analysis of solids with more general constitutive laws under high rates of loading, according to which one seeks the solid's fastest growing eigenmode, or the wavelength associated with lowest necking strain. This method has been repeatedly applied in the study of dynamic stability of elastoplastic bars and rings under high loading rates where the size of fragments is of interest (e.g. see Shenoy and Freund, 1999; Sorensen and Freund, 2000; Guduru and Freund, 2002; Mercier and Molinari, 2003; Zhou et al., 2006; Xue et al., 2008). However, recent

* Corresponding author at: Laboratoire de Mécanique des Solides & Département de Mécanique, École Polytechnique, Palaiseau 91128, France.
E-mail addresses: kravi@mail.utexas.edu (K. Ravi-Chandar), nick@lms.polytechnique.fr (N. Triantafyllidis).

http://dx.doi.org/10.1016/j.ijsolstr.2014.09.015
0020-7683/

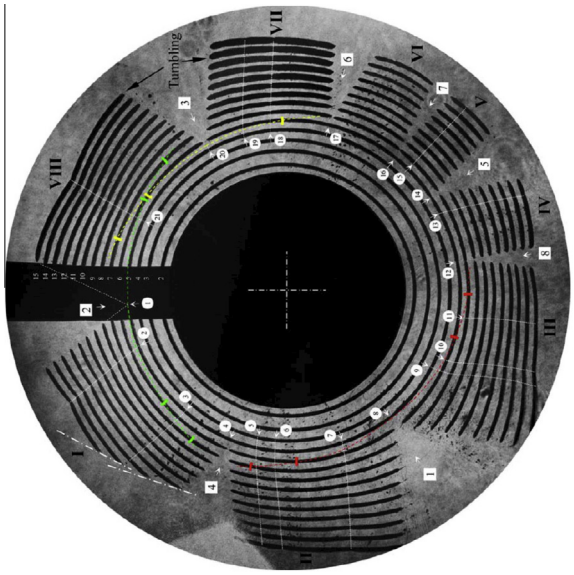

Fig. 1. Composite image for an electromagnetically expanding Al 6061-O thin ring test (from Zhang and Ravi-Chandar, 2006), showing the onset and evolution of necks under high strain rate loading; see reference for detailed interpretation.

experimental evidence from rapidly expanding electromagnetically loaded metallic rings by Zhang and Ravi-Chandar (2006, 2008) finds no evidence of a dominant wavelength at the necked pattern of the rings, as seen in the unbroken configuration of the ring in Fig. 1. Moreover, they find no experimental evidence of influence of strain rate on the necking strains, which are consistent with maximum force criterion of a rate independent constitutive law (Considère criterion).

As explained by these authors, using the fastest growing eigenmode to predict the onset of failure is physically meaningful provided that some characteristic velocity of the principal solution – e.g. ring expansion rate – is much slower than the speed of propagation of perturbations in the solid or structure at hand. For high loading rates, commensurate with some characteristic wave propagation speed in the structure, a novel approach to the stability analysis is required, namely the study of evolution of localized perturbations.

For the above reasons, we investigate here the evolution of spatially localized perturbations in a nonlinearly elastic bar at arbitrary strain rates when inertia is taken into account. Given the adequacy of a rate-independent constitutive model and the absence of unloading at any point in the bar until necking strain is reached – because of the background strain rate of the principal solution, loading conditions prevail at all points up to Considère strain – nonlinear elasticity is an adequate model for rate-independent elastoplasticity. The problem formulation is given in Section 2, followed by the results in Section 3 and ending with a conclusion in Section 4. A linearized stability analysis for the case of a viscoplastic constitutive model is given in the Appendix A.

2. Problem formulation

The problem formulation section starts with the presentation of the model for the dynamically loaded 1D bar followed by the description of two different stability criteria: the new one based on the evolution of a spatially localized perturbation and, for comparison, the classical one based on modal analysis to determine the fastest growing eigenmode. The linearized analysis of the bar stability problem using these two criteria comes next, followed by a description of the algorithm used for the calculations of the associated nonlinear dynamics problem.

2.1. Model

We consider a 1D bar of uniform cross-sectional area A in the reference and a in the current configuration.[1] We further assume the bar to be incompressible, in which case its logarithmic strain ϵ is given in terms of the stretch ratio λ by:

$$\epsilon \equiv \ln \lambda, \quad \lambda \equiv dx/dX = A/a, \tag{2.1}$$

where X and x are respectively the reference and current configuration axial coordinates of the bar.

The spatially constant 1st Piola–Kirchhoff stress of the bar Π (force/reference area) can be expressed in terms of its Cauchy stress σ with the help of (2.1) by:

$$\Pi = \sigma(a/A) = \sigma \exp(-\epsilon). \tag{2.2}$$

The reference configuration equation of motion of the 1D bar is given by:

$$\frac{\partial \Pi}{\partial X} = \rho \frac{\partial v}{\partial t}, \tag{2.3}$$

where v is the particle velocity of the material point X. Combining the kinematics (2.1) and stress relations (2.2) with the equation of motion (2.3) we obtain the following system of governing equations for the bar in terms of its strain ϵ and particle velocity v:

$$\begin{aligned} \frac{\partial \epsilon}{\partial t} &= \exp(-\epsilon)\frac{\partial v}{\partial X}, \\ \frac{\partial v}{\partial t} &= \exp(-\epsilon)[(\sigma_{,\epsilon} - \sigma)/\rho]\frac{\partial \epsilon}{\partial X}, \end{aligned} \tag{2.4}$$

where $\sigma_{,\epsilon} \equiv d\sigma/d\epsilon$; a nonlinear constitutive law $\sigma(\epsilon)$ is to be subsequently satisfied.

The perfect bar is subjected to a uniform stretch rate $c \equiv d\lambda_0/dt$. Denoting the associated field quantities by a subscript $()_0$, the principal solution of the bar, whose stability is to be investigated here, is given by:

$$\lambda_0 = 1 + ct; \quad \epsilon_0 = \ln(1 + ct), \ v_0 = cX. \tag{2.5}$$

Although the 1D bar model introduced above is valid for any material, discussing the features of the constitutive laws pertaining to the associated characteristic wave propagation speeds is in order at this point. The characteristics of the above hyperbolic system (2.4) of equations are found by looking for solutions of the type: $\epsilon = C_\epsilon f(X \pm Vt)$, $v = C_v f(X \pm Vt)$ where C_ϵ, C_v are constants and $f(z)$ an arbitrary function. It follows from (2.4) that the characteristic speed V of the system is[2]:

$$V = \exp(-\epsilon)[(\sigma_{,\epsilon} - \sigma)/\rho]^{1/2}. \tag{2.6}$$

For as long as $\sigma_{,\epsilon} - \sigma > 0$ disturbances propagate at a finite speed V given by (2.6). The condition $\sigma_{,\epsilon} - \sigma = 0$, which as seen from (2.2) corresponds to a maximum force (Considère criterion $d\Pi/d\epsilon = 0$), signals the onset of necking at the strain that satisfies this condition. The uniaxial loading curve of most structural metals does reach a maximum force and hence constitutive laws for which a realistic strain ϵ_m, termed *Considère strain* or equivalently *necking strain* exists such that:

$$\sigma_{,\epsilon}(\epsilon_m) - \sigma(\epsilon_m) = 0, \tag{2.7}$$

[1] Here and subsequently reference configuration quantities are denoted by an upper case symbol while their current configuration counterparts are denoted by the corresponding lower case symbol.

[2] The coefficient $\exp(-\epsilon) = \lambda$ appears in (2.6) because the characteristic speed V pertains to the reference configuration; the characteristic speed in the current configuration is $[(\sigma_{,\epsilon} - \sigma)/\rho]^{1/2}$.

will be considered. Once ϵ_m has been reached in the bar, an unloading wave can start from this point resulting in the formation of a neck discontinuity and the bar can no longer deform uniformly as described in (2.5).

In this work we are interested in the stability of the bar's principal (uniform strain) solution (2.5) for strains $\epsilon < \epsilon_m$. Since no unloading occurs in the bar for these strains, the use of a nonlinear constitutive model characterized by $\sigma(\epsilon)$ is adequate for analyzing its stability.

2.2. Linearized stability analyses

In order to get an analytically tractable way to investigate the stability of the bar's uniform strain solution (2.5), we start by studying the linearized system for the evolution of a perturbation in (2.4). By defining the strain and particle velocity perturbations as:

$$\delta\epsilon(X,t) \equiv \epsilon(X,t) - \epsilon_0(t), \quad \delta v(X,t) \equiv v(X,t) - v_0(X) \tag{2.8}$$

and introducing them to (2.4) one obtains upon linearization about the uniform strain solution (2.5) the following system:

$$\begin{aligned} \frac{\partial \delta v}{\partial X} &= \exp(\epsilon_0)\left(\frac{\partial \delta\epsilon}{\partial t} + \frac{d\epsilon_0}{dt}\delta\epsilon\right), \\ \frac{\partial \delta v}{\partial t} &= \exp(-\epsilon_0)\left[\frac{\sigma_{,\epsilon}(\epsilon_0) - \sigma(\epsilon_0)}{\rho}\right]\frac{\partial \delta\epsilon}{\partial X}. \end{aligned} \tag{2.9}$$

By eliminating δv from the above system, one obtains the following linear equation for the evolution of the strain perturbation $\delta\epsilon$:

$$\frac{\partial^2 \delta\epsilon}{\partial t^2} + \frac{2c}{1+ct}\frac{\partial \delta\epsilon}{\partial t} - \frac{1}{(1+ct)^2}\left[\frac{\sigma_{,\epsilon}(\epsilon_0) - \sigma(\epsilon_0)}{\rho}\right]\frac{\partial^2 \delta\epsilon}{\partial X^2} = 0, \tag{2.10}$$

to which initial conditions for $\delta\epsilon$ and $\partial\delta\epsilon/\partial t$ must be added. A completely equivalent formulation of the problem could have been obtained for the particle velocity perturbation δv.

Since perturbations travel at a finite speed $V(\epsilon)$ according to (2.6), it makes sense to follow the evolution of a spatially localized perturbation, its physical motivation being the appearance at time t_0 of a local defect. We thus consider two different cases: (i) a strain rate (or equivalently from (2.4) a particle velocity) perturbation and (ii) a strain perturbation.

2.2.1. Localized particle velocity perturbation

The initial conditions for (2.10) in this case are assumed to be:

$$\delta\epsilon(X,t_0) = 0, \quad \frac{\partial \delta\epsilon}{\partial t}(X,t_0) = \delta_D(X), \tag{2.11}$$

where $\delta_D(X)$ is the Dirac delta function.

Solving analytically for the time-dependent coefficients in the strain perturbation equation (2.10) is a rather difficult task. Since we are interested in following the initial evolution of the perturbation near time t_0 we can neglect the time-dependence of its coefficients (method of frozen coefficients). In this case (2.10) with initial conditions (2.11) becomes analytically tractable and is solved with the help of a Laplace transform. Using the symbol $\widetilde{f}(X,s)$ to denote the Laplace transform with respect to time of $f(X,t)$, one obtains:

$$(s^2 + \beta s)\widetilde{\delta\epsilon} - V^2\frac{\partial^2 \widetilde{\delta\epsilon}}{\partial X^2} = \delta_D(X); \quad \beta \equiv \frac{2c}{1+ct_0}, \tag{2.12}$$

which gives the following result for the Laplace transform $\widetilde{\delta\epsilon}(X,s)$:

$$\widetilde{\delta\epsilon}(X,s) = \frac{1}{2V\sqrt{s^2+\beta s}}\left[(1-H(X))\exp[(X/V)\sqrt{s^2+\beta s}] + H(X)\exp[-(X/V)\sqrt{s^2+\beta s}]\right], \tag{2.13}$$

where $H(X)$ is the Heaviside function.

The bar is stable if its initial perturbation in (2.11) decays for large times. A fast way to investigate the behavior of $\delta\epsilon(X,t)$ as $t \longrightarrow \infty$ is by use of Abel's theorem that states:

$$\lim_{t\longrightarrow\infty} \delta\epsilon(X,t) = \lim_{s\longrightarrow 0} s[\widetilde{\delta\epsilon}(X,s)]. \tag{2.14}$$

From (2.13) we obtain:

$$\lim_{s\longrightarrow 0} s[\widetilde{\delta\epsilon}(X,s)] = \lim_{s\longrightarrow 0}\frac{s}{2V\sqrt{s^2+\beta s}} = 0 = \lim_{t\longrightarrow\infty}\delta\epsilon(X,t) \tag{2.15}$$

and the above results shows that for times near the onset of perturbation time t_0 the perturbation decays.

One can also invert the Laplace transform $\widetilde{\delta\epsilon}(X,s)$ to calculate $\delta\epsilon(X,t)$, which is a symmetric function of X. For $X \geqslant 0$ one obtains by inversion of (2.13):

$$\begin{aligned} &\delta\epsilon(X,t) = \frac{1}{2V}\exp[-(\beta/2)\Delta t]\, I_0[(\beta/2)t_m]\, H[t_f], \\ &\text{using}: \Delta t \equiv t - t_0, \quad t_f \equiv \Delta t - (X/V), \quad t_b \equiv \Delta t + (X/V), \quad t_m \equiv \sqrt{t_f t_b}, \end{aligned} \tag{2.16}$$

where t_f and t_b are respectively the forward and backward retardation times and $I_0(z)$ – a monotonically increasing function of its argument – is the modified Bessel function of order zero that is regular at the origin ($I_0(0) = 1$). It can be seen that the perturbation $\delta\epsilon$ spreads over the interval $[-(t-t_0)V, (t-t_0)V]$ with a decreasing maximum amplitude – which is always located at $X = 0$ – which confirms the result of (2.15) that at times near t_0 the bar is stable under a local perturbation.

2.2.2. Localized strain perturbation

The initial conditions for (2.10) in this case are:

$$\delta\epsilon(X,t_0) = \delta_D(X), \quad \frac{\partial \delta\epsilon}{\partial t}(X,t_0) = 0 \tag{2.17}$$

and hence the Laplace transform of (2.10) with initial conditions (2.17) gives:

$$(s^2 + \beta s)\widetilde{\delta\epsilon} - V^2\frac{\partial^2 \widetilde{\delta\epsilon}}{\partial X^2} = (s+\beta)\delta_D(X); \quad \beta \equiv \frac{2c}{1+ct_0}. \tag{2.18}$$

The solution of the above equation is found to be:

$$\widetilde{\delta\epsilon}(X,s) = \frac{(s+\beta)}{2V\sqrt{s^2+\beta s}}\left[(1-H(X))\exp[(X/V)\sqrt{s^2+\beta s}] + H(X)\exp[-(X/V)\sqrt{s^2+\beta s}]\right]. \tag{2.19}$$

Once again the application of Abel's theorem shows as in (2.15) that for times near the onset of perturbation time t_0 the perturbation decays.

Inverting $\widetilde{\delta\epsilon}(X,s)$ in (2.19) to obtain $\delta\epsilon(X,t)$, which is a symmetric function of X, one has for $X \geqslant 0$:

$$\delta\epsilon(X,t) = \frac{1}{2V}\exp[-(\beta/2)\Delta t]\left\{\left[I_0[(\beta/2)t_m] + \frac{\Delta t}{t_m}I_1[(\beta/2)t_m]\right]\frac{\beta}{2}H[t_f] + \delta_D(t_f)\right\}, \tag{2.20}$$

where the definitions of t_f, t_b, t_m are given in (2.16) and $I_1(z) = dI_0(z)/dz$ is the modified Bessel function of order one that is regular at the origin ($I_1(0) = 0$). In contrast to the particle velocity perturbation case in (2.16) we now have the strain singularity introduced at $X = 0$ at time t_0 splitting in two and propagating at the wavefronts $X = \pm V\Delta t$ but with an exponentially decaying strength.

The above linearized perturbation analysis shows that as long as the perturbation occurs at a time for which the strain in the bar is less than the Considère strain ($\epsilon_0 < \epsilon_m$ or equivalently from (2.6) the characteristic speed $V > 0$), the bar is – at least initially, near t_0 – stable to spatially localized perturbations (an arbitrary

perturbation is obtained by superposition of the Green solutions given above).

2.2.3. Modal analysis

It is worth noticing that the modal analysis of the perturbation gives the same linearized result. The proof of this assertion is straightforward and proceeds as follows: Consider a strain perturbation of the form:

$$\delta\epsilon(X,t) = \alpha \exp(ikX + \eta t), \tag{2.21}$$

where k is the wavenumber of the perturbation, α its amplitude, η the corresponding growth rate, and i the imaginary unit. Upon introducing (2.21) into the perturbation equation (2.10), and ignoring again the time-dependence of its coefficients, one obtains the following equation for η:

$$\eta^2 + \frac{2c}{1+ct_0}\eta + (kV)^2 = 0 \quad \Rightarrow \quad \eta = \frac{1}{1+ct_0}\left\{-c \pm [c^2 - k^2(\sigma_\epsilon - \sigma)/\rho]^{1/2}\right\}, \tag{2.22}$$

which clearly shows linearized stability for $\sigma_\epsilon - \sigma > 0$ since both roots of (2.22) are either negative or have a negative real part.

2.3. Nonlinear dynamics calculations

If we define the Riemann variables $R_\pm = \mp v + V\epsilon$, then $dR_\pm = \mp dv + Vd\epsilon = 0$ on $dX = \pm Vdt$. For given initial conditions, the governing equations (2.4) can be used incrementally to march in time. However, because V depends on ϵ, the characteristics should be updated at every time step. In implementing this method, we divide X-axis into discrete nodes and time into a series of time steps. Let X_i^k denote the node at i at time-step k. The time increment at each step is calculated such that the fastest wave speed from the previous time step satisfies the Courant–Friedrichs–Levy condition. In addition, X_-^k is the origin of the characteristic $-V_-^k$, that arrives at X_i^{k+1}, and is located between nodes X_i^k and X_{i+1}^k; similarly, X_+^k is the origin of the characteristic, V_+^k, that arrives at X_i^{k+1} and is located between nodes X_{i-1}^k and X_i^k. These characteristics are found by interpolation at time step k; this method is a variant of the scheme commonly called upwind differencing in fluid mechanics.

The above-described procedure can be used to perform a full numerical solution of the dynamic problem. In particular, if a perturbation of the type indicated in (2.8) is applied at some time t_0 on a background uniform strain-rate expansion, the spatio-temporal evolution of the perturbation can be evaluated without resorting to the frozen coefficient approach of the linear stability analysis described in Section 2.2. Results from such an analysis of the stability are described in the next section.

3. Results

This section starts with the constitutive model chosen and continues with the definitions of the dimensionless time: τ and space: χ variables that are used in plotting the results. The study of the evolution of a single spatially localized perturbation with different amplitudes and initial times is presented next, followed by the study on interaction of two or more such perturbations, leading to an explanation of the localized failure patterns observed experimentally in Zhang and Ravi-Chandar (2006).

3.1. Constitutive law, non-dimensionalization and perturbation profile

The analysis in Section 2 is perfectly general; any nonlinear constitutive law can be accommodated provided that it has a necking strain (maximum force). In the results presented here the simplest such choice will be made, namely a simple power-law relation between the Cauchy stress σ and the logarithmic strain ϵ:

$$\sigma = K\epsilon^n, \tag{3.1}$$

where K is a material constant and n the hardening exponent. In the subsequent numerical calculations $n = 0.22$, which is a reasonable value for the aluminum alloys used in the experiments of Zhang and Ravi-Chandar (2006). For this particular constitutive choice, the necking strain ϵ_m is found by using (3.1) into (2.7) to be: $\epsilon_m = n = 0.22$.

The profile of the spatially localized numerical perturbations used in calculations is:

$$\delta\epsilon(X,t_0) \text{ or } \delta v(X,t_0) = \alpha\,[\tanh(\xi X + \zeta)) - \tanh(\xi X - \zeta)], \tag{3.2}$$

where α is the amplitude, ξ is the shape-controlling parameter and 2ζ is the width of a perturbation localized about $X = 0$.

In the presentation of results, we use the following dimensionless quantities for time and length:

$$\text{dimensionless time}: \tau \equiv ct, \quad \text{dimensionless length}: \chi \equiv Xc/\sqrt{K/\rho}. \tag{3.3}$$

3.2. Evolution of spatially localized perturbations

We start by analyzing the evolution of a single spatially localized strain perturbation at $\chi = 0$ introduced at a very small (near yield) strain, i.e. at a dimensionless time $\tau_0 = 0.0015$ and amplitude $\alpha = \pm 0.01$ as seen in Fig. 2, which depicts the strain of the bar as a function of position taken at equal time increments.

The strain perturbation amplitude initially decays, as predicted by the linearized analysis in Section 2.2. The perturbation then splits into two parts, each traveling in opposite direction from the other at a speed that decreases with strain, as expected from (2.6) and (3.1). In Fig. 2 we also indicate by the asterisk symbol ($*$) the shadow cone of the origin $\pm\int_0^\epsilon [(\sigma_\epsilon - \sigma)/\rho]^{1/2} d\epsilon$ that separates the perturbed from the unperturbed regions of the bar. The maximum strain in each one of the localized strain zones subsequently increases until the necking strain is reached (at two symmetric with respect to the origin locations) and calculation is stopped.

Notice that the positive amplitude $\alpha > 0$ strain perturbation reaches the necking strain slightly earlier than its negative amplitude $\alpha < 0$ counterpart, as seen by the difference in the strains of the unperturbed part of the bar. Also observe that the distance between the two maximum strain locations is smaller in the latter case and about half the size predicted by the shadow cone.

To better illustrate the evolution of a localized perturbation, we plot in Fig. 3 the contours in the perturbation of particle velocity with the same amplitudes, location and initial time as in Fig. 2.

The results depicted in Fig. 3 show that the particle velocity perturbation initially decays (its amplitude decreases) as it splits into two parts that travel with progressively slower speeds. Each one of these two localized perturbations become pinned in space and subsequently grow in amplitude until the necking strain is reached.

A separate calculation was done by following the evolution of a single spatially localized velocity perturbation introduced at a very small strain; the results are similar to those obtained with the single spatially localized strain perturbation and are therefore not shown here.

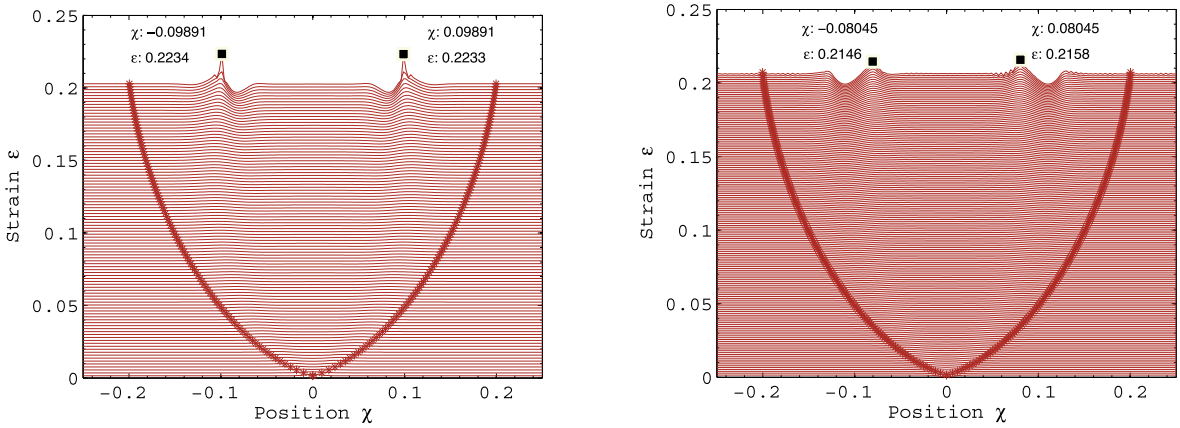

Fig. 2. Growth of a strain perturbation, starting at $\tau_0 = 0.0015$, of amplitude $\alpha = 0.01$ (left) and $\alpha = -0.01$ (right). The shadow cone – region of influence of the disturbance calculated from the strain-dependent perturbation speed $V(\epsilon)$ – is indicated by the asterisk symbol $(*)$.

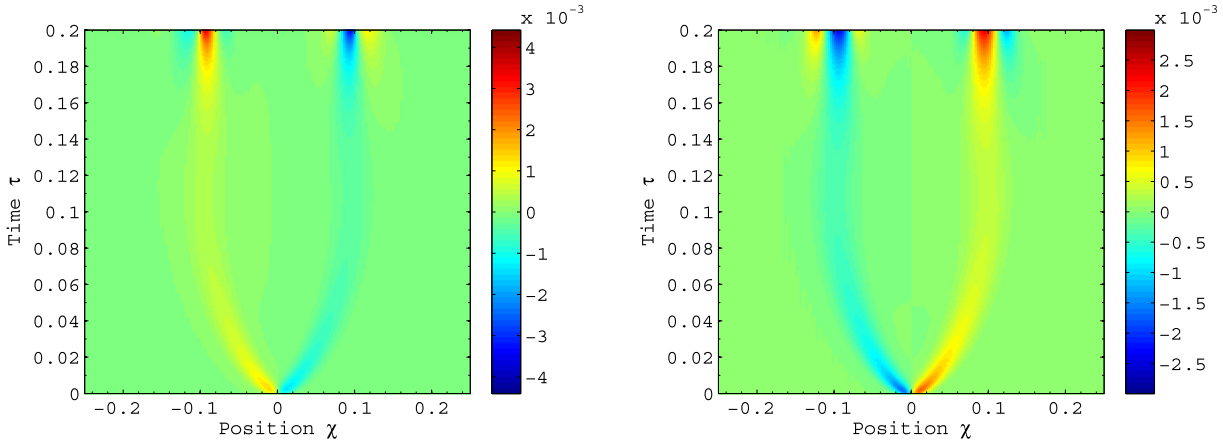

Fig. 3. Contours showing the normalized particle velocity perturbation following the introduction of a strain perturbation at $\tau_0 = 0.0015$. of amplitude $\alpha = 0.01$ (left) and $\alpha = -0.01$ (right).

The influence of the perturbation amplitude α is investigated next in Fig. 4, which shows that the strain of a bar subjected to two perturbations localized at $\chi = 0$: one with a small amplitude $\alpha = 0.001$ (left) and one with a large amplitude $\alpha = 0.05$ (right). The strain perturbation is again introduced at dimensionless time $\tau_0 = 0.0015$ (same as in the preceding calculations in Figs. 2 and 3) and is plotted as a function of position taken at equal time increments. Although the same behavior as in Fig. 2 is observed, namely the perturbation splits in two parts that subsequently propagate at decreasing speed but increasing amplitude, the bar with smaller initial perturbation amplitude necks, i.e. reaches its Considère strain, significantly later than the one with its larger counterpart; the strain in the unperturbed part of the bar when necking is reached for the small amplitude perturbation $\alpha = 0.001$ is close

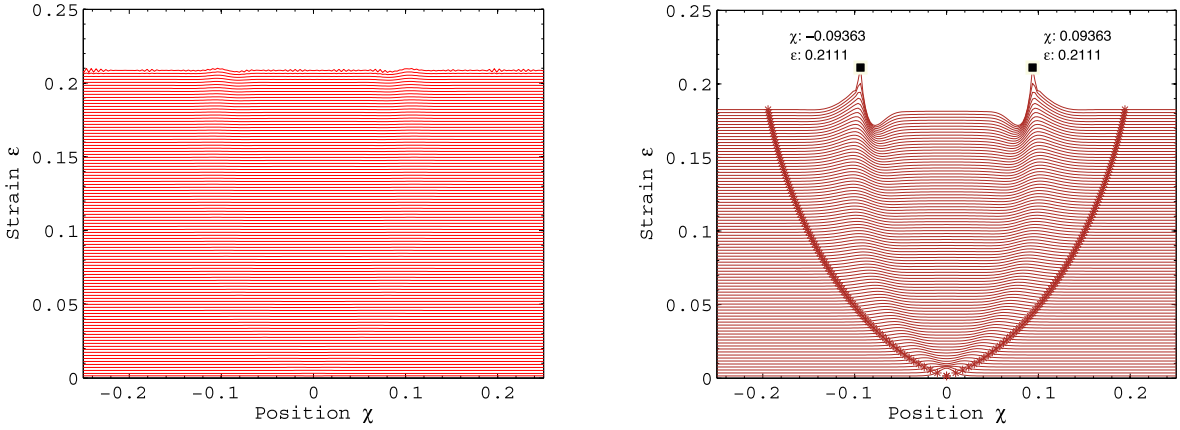

Fig. 4. Influence of the initial amplitude of a strain perturbation starting at $\tau_0 = 0.0015$. Notice that a state of almost uniform strain persists almost near the Considère strain for a perturbation of small amplitude $\alpha = 0.001$ (left) while a strongly nonuniform strain develops much earlier for perturbations of large amplitude $\alpha = 0.05$ (right).

to the necking strain $\epsilon = 0.22$ of the bar, while the strain in the unperturbed part of the bar when necking is reached for the large amplitude perturbation $\alpha = 0.001$ is $\epsilon = 0.18$.

The results in Fig. 4 show the stability of the bar to spatially localized perturbations up to necking (reaching ϵ_m in at least one location): The smaller the amplitude of the initial perturbation, the smaller the final maximum amplitude of the perturbation when necking of the bar is reached. This is a much stronger nonlinear stability result that complements the linearized stability analysis in Section 2.2.

The influence of the onset of perturbation time is examined in Fig. 5, which shows the strain profiles of the bar at regular time intervals, for spatially localized perturbations of amplitude $\alpha = 0.01$; one starting earlier at time $\tau_0 = 0.015$ (left) and the other starting later at $\tau_0 = 0.15$ (right). The evolution of the perturbation starting earlier proceeds like the ones in Figs. 2 and 4, i.e. the initially localized at $\chi = 0$ perturbation splits in two parts that subsequently propagate at decreasing speed but increasing amplitude. In contrast, the evolution of the perturbation that starts later at $\tau_0 = 0.15$ does not have sufficient time to split in two but continues to grow in amplitude until necking is reached at the same location it was introduced, i.e. $\chi = 0$. In comparing Figs. 2 and 5, we see that the distance between necking locations is reduced as the time of initial perturbation gets delayed, as expected from the decreasing shadow cone of the delayed perturbation.

The above results, all of which pertain to a single spatially localized perturbation, suggest the basic mechanism of failure of the bar under high strain rates: the interaction of perturbations evolving from different imperfection sites in the bar. The solution to the rapidly strained bar with a multitude of statistically distributed and triggered imperfections leads to a configuration with multiple necks, as seen in Fig. 1. Therefore, we investigate the interaction of two or more perturbations placed along the length of the bar. These results are described next.

The interaction of two spatially localized strain perturbations of the same amplitude $\alpha = 0.01$, both starting at $\tau_0 = 0.0015$, are shown in Fig. 6. To ensure interaction, the two perturbations in Fig. 6 are placed at a distance smaller than the final shadow cone corresponding to a single perturbation starting at $\tau_0 = 0.0015$, resulting in four local strain maxima near ϵ_m. Notice that the smaller spacing between these strain maxima is lower than the spacing between the two strain maxima of the single perturbation seen in Fig. 2. Moreover, the spacing of the two largest strain maxima exceeds the corresponding spacing for the single perturbation case.

Additional simulations were performed for cases in which the two imperfections were spatially and temporally separated from

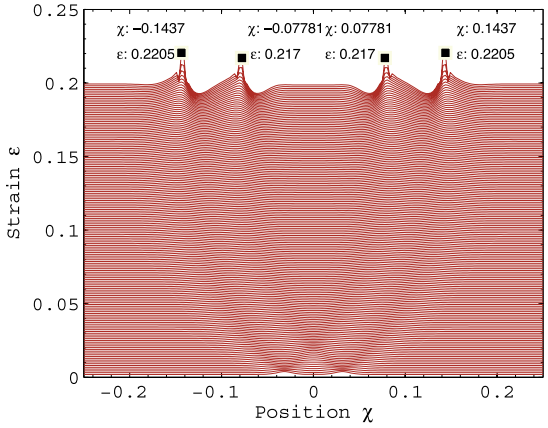

Fig. 6. Interaction of two strain perturbations of same amplitude $\alpha = 0.01$ starting at $\tau_0 = 0.0015$. Notice the strain pattern when necking is reached: the distance between maximum strain locations is shorter than the one in Fig. 2, calculated for a single perturbation.

each other; in all cases, the interaction between the two imperfections causes a strain pattern in which the eventual spacing between necks is smaller than in the case of the isolated imperfection which is activated near zero strain. One final set of simulations was performed where a number of defects (between 5 and 30) were distributed at random along the length of the bar; the locations were determined by a random sequence generator in MATLAB and the amplitude was assigned the range $\alpha \in [-0.01, 0.01]$, determined by another random number sequence. The entire set of perturbations was again introduced at time $\tau_0 = .0015$, thus simulating initial defects. Results of these calculations are depicted in Fig. 7, with the left figure corresponding to a bar having 10 imperfection sites while on the right the bar has 30 imperfection sites.

These perturbations also indicate an initial decay, and eventual growth as the mean strain approaches the Considère strain, ϵ_m. The pattern of eventual neck development from these random perturbations could only set a lower bound for the neck free length in the following sense: since the bar has potentially a large number of imperfections, it is the one with the largest amplitude that is activated as soon as the bar is strained that will form the shadow cone that will reach first the Considère strain. As seen from the calculations in Fig. 7 the minimum neck spacing is associated with the non-interacting perturbations of the largest amplitude. Given the nonlinear nature of the problem, the correct calculation of this

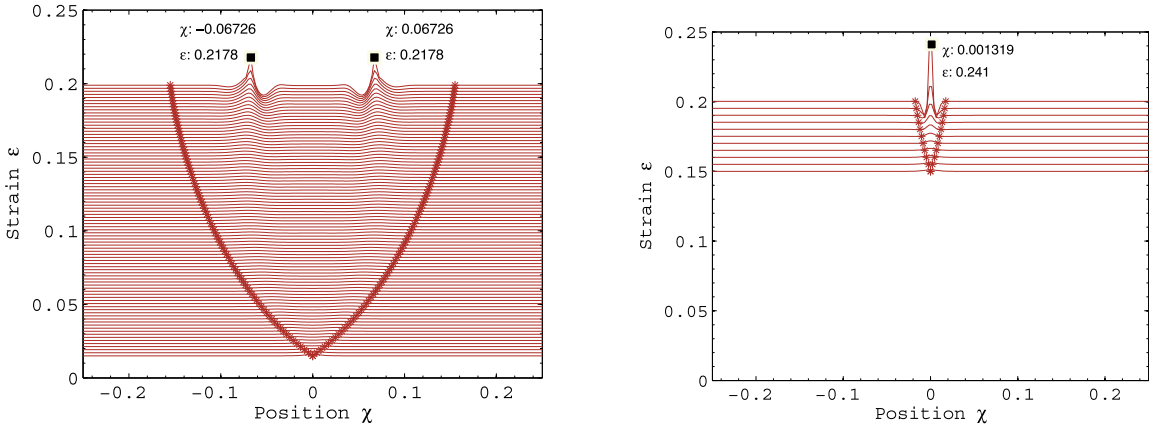

Fig. 5. Influence of the time of onset for a perturbation of amplitude $\alpha = 0.01$. Notice that the perturbation starting earlier at $\tau_0 = 0.015$ (left) has two strain maxima while the perturbation starting later at $\tau_0 = 0.15$ (right) results in only one strain maximum.

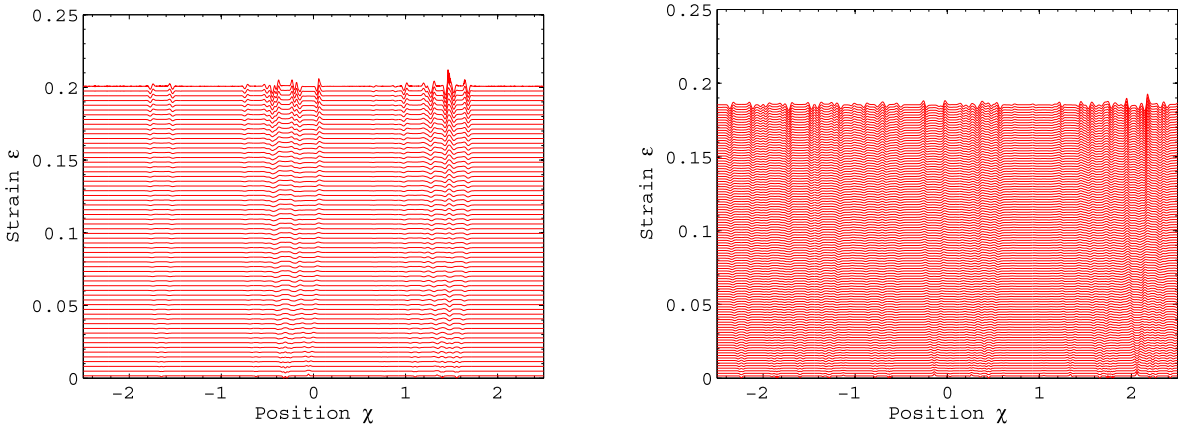

Fig. 7. Influence of randomly distributed perturbations of maximum amplitude $\alpha = 0.01$ starting near zero strain ($\tau_0 = 0.015$). On the left the bar has 10 imperfection sites while on the right the bar has 30 imperfection sites.

length cannot be done analytically, but can be found numerically from the evolution of the single perturbation, as discussed in Fig. 2.

4. Conclusion

This work pertains to the influence of loading rate on the stability of structures when inertia plays a dominant role. The currently established approach to study these stability problems is the method of modal analysis, which determines the structure's fastest growing eigenmode. This method supposes that all points in the structure can be perturbed simultaneously, an assumption that is not appropriate for cases when the velocity of material points in the structure are comparable to the associated wave propagation speeds.

The novel idea here is to analyze the evolution of spatially localized perturbations of the time-dependent, high-strain-rates states of these structures, in order to understand the initiation of the corresponding failure mechanisms. In the interest of (relative) simplicity, we study the high strain extension of a 1D, incompressible, nonlinearly elastic bar. Using a nonlinear constitutive law makes sense for real structures since no unloading occurs until a point in the structure reaches the bar's necking strain ϵ_m, at which point our calculations are terminated. The adequacy of our constitutive assumption is further supported by the experimental evidence from Zhang and Ravi-Chandar (2006), who find that the onset of necking strains is consistent with the maximum force criterion (2.7) and independent of the applied strain rates (no viscoplasticity effects).

It is shown here that the bar is stable to localized perturbations as long as all points in the bar have strains below ϵ_m. Stability is established by linearized analysis and also by a full nonlinear analysis. Both methods show that the maximum amplitude of a spatially localized perturbation decreases with decreasing amplitude of the initial perturbation, provided of course that no point in the bar has reached ϵ_m. The same linearized stability result is shown in Appendix A to hold even in the case of viscoplasticity.

Our analysis also provides a consistent explanation for the necking patterns obtained in the high strain-rate extension experiments of thin rings by Zhang and Ravi-Chandar (2006), which show the absence of a dominant wavelength, in contrast of the theoretical predictions based on modal analysis arguments. The experimentally observed random spacing between necks is dictated by the presence of inevitable imperfections that are sources of perturbations for the perfect bar subjected to a given extension rate. The interactions of these perturbations indicate that the maximum distance between necks is the maximum size of the (nonlinear) shadow cone at the onset of necking of any point in the bar corresponding to a perturbation initiated at the onset of deformation. Since the distance between the two strain maxima of a localized defect reached at Considère strain diminishes with the strain at the onset of perturbation (see discussion of Fig. 5), the minimum distance between necks cannot be found from this model and is expected to be of the order of the bar thickness thus requiring a higher geometric dimension analysis for its determination. It is also noteworthy that since the size of the actual shadow cone of a localized defect depends on the applied strain rate – see definition of dimensionless length in (3.3) – the minimum distance between necks should diminish with strain rate, as observed experimentally by Zhang and Ravi-Chandar (2006).

The above approach is useful for the stability analysis of more realistic structures under high strain rates. As one such example we cite the recent work by Putelat and Triantafyllidis (2014) on the stability of a pressurized thin ring at high rates, where it is shown that for small values of the applied loading rate, the structure fails through a global mode, while for large values of the applied loading rate the structure fails by a localized mode of deformation, as also found recently in the experiments of Mainy and Ravi-Chandar (submitted for publication). However useful, the 1D model used here has its limitations, thus motivating a higher geometric dimension analysis of the problem and inclusion of unloading.

Acknowledgments

The authors acknowledges support through a collaborative grant from the US National Science Foundation, Grants CMMI-0900293 (K. R.) and CMMI-0900007 (N. T.). This work has been conducted during the first author's sabbatical leave at the Solid Mechanics Laboratory of the École Polytechnique during the Academic Year 2011–2012, made possible through the generosity of the École Polytechnique and the CNRS. This support is gratefully acknowledged.

Appendix A. Stability of a viscoplastic bar

Since the stability analysis of viscoplastic bars under high strain rates has been frequently studied in the past, it is worth revisiting this issue to investigate the response of viscoplastic bars to spatially localized perturbations.

Once again we start with the kinematics (2.1), (2.2)and equations of motion (2.3) to which we add the constitutive law, a

simple overstress model, thus resulting in the following system of equations:

$$\begin{aligned}
&\exp(\epsilon)\frac{\partial \epsilon}{\partial t} = \frac{\partial v}{\partial X},\\
&\frac{\partial[\sigma\exp(-\epsilon)]}{\partial X} = \rho\frac{\partial v}{\partial t},\\
&\sigma = E(\epsilon - \epsilon^p),\\
&\frac{\partial \epsilon^p}{\partial t} = \frac{1}{\zeta}[\sigma - g(\epsilon)],
\end{aligned} \tag{A.1}$$

where ϵ^p is the plastic part of the strain, ζ is the viscosity and $g(\epsilon^p)$ is the hardening function of the accumulated plastic strain.

Introducing into the above equations perturbations about the uniform rate solution (2.5), one obtains upon linearization:

$$\begin{aligned}
&\frac{\partial \delta v}{\partial X} = \exp(\epsilon_0)\left(\frac{\partial \delta\epsilon}{\partial t} + \frac{d\epsilon_0}{dt}\delta\epsilon\right),\\
&\rho\frac{\partial \delta v}{\partial t} = \exp(-\epsilon_0)\left[(E-\sigma_0)\frac{\partial \delta\epsilon}{\partial X} - E\frac{\partial \delta\epsilon^p}{\partial X}\right],\\
&\frac{\partial \delta\epsilon^p}{\partial t} = \frac{1}{\zeta}\left[E(\delta\epsilon - \delta\epsilon^p) - \frac{dg}{d\epsilon^p}\delta\epsilon^p\right],
\end{aligned} \tag{A.2}$$

where all the coefficients of the above equation are evaluated on the uniform rate solution.

By differentiating the first equation in (A.2) with respect to time and the second with respect to space to eliminate δv and rearranging the third, one obtains the following relation between $\delta\epsilon$ and $\delta\epsilon^p$:

$$\begin{aligned}
&\frac{\partial^2 \delta\epsilon}{\partial t^2} + \frac{2c}{1+ct}\frac{\partial \delta\epsilon}{\partial t} - \frac{E-\sigma_0}{\rho(1+ct)^2}\frac{\partial^2 \delta\epsilon}{\partial X^2} + \frac{E}{\rho(1+ct)^2}\frac{\partial^2 \delta\epsilon^p}{\partial X^2} = 0,\\
&\zeta\frac{\partial \delta\epsilon^p}{\partial t} - E\delta\epsilon + \left(E + \frac{dg}{d\epsilon^p}\right)\delta\epsilon^p = 0.
\end{aligned} \tag{A.3}$$

To the above system, one has to add the initial conditions:

$$\delta\epsilon(X,t_0) = \Delta\epsilon_0(X), \quad \frac{\partial \delta\epsilon}{\partial t}(X,t_0) = \Delta\epsilon_1(X) \quad \delta\epsilon^p(X,t_0) = 0, \tag{A.4}$$

since in perturbing a viscoplastic solid we cannot directly control the internal variable $\delta\epsilon^p$ (see discussion in Nestorovic et al. (2000)).

As for the case of the linearized stability analysis of the nonlinear bar in Section 2.2, we find it easier to work with the Laplace transforms of the independent variables $\widetilde{\delta\epsilon}$ and $\widetilde{\delta\epsilon^p}$. In taking the Laplace transforms of (A.3) together with the initial conditions (A.4) and eliminating $\widetilde{\delta\epsilon^p}$ we obtain the following expression for $\widetilde{\delta\epsilon}$:

$$\begin{aligned}
&(s^2+\beta s)\widetilde{\delta\epsilon} - \frac{E}{\rho(1+ct_0)^2}\left[1 - \frac{\sigma_0}{E} - \frac{E}{\zeta s + E + dg/d\epsilon_p}\right]\frac{\partial^2 \widetilde{\delta\epsilon}}{\partial X^2}\\
&\quad = (s+\beta)\Delta\epsilon_0 + \Delta\epsilon_1; \quad \beta \equiv \frac{2c}{1+ct_0}.
\end{aligned} \tag{A.5}$$

Similarly to the rate-independent bar case in (2.12) and (2.18), in order to have time-decaying solutions for the strain perturbation, the coefficient of $\partial^2\widetilde{\delta\epsilon}/\partial X^2$ in (A.5) must be positive:

$$\left[1 - \frac{\sigma_0}{E} - \frac{E}{\zeta s + E + dg/d\epsilon_p}\right] > 0. \tag{A.6}$$

Since $\zeta s > 0$, one has from (A.6) the following inequality:

$$\begin{aligned}
1 - \frac{\sigma_0}{E} - \frac{E}{\zeta s + E + dg/d\epsilon_p} &> 1 - \frac{\sigma_0}{E} - \frac{E}{E + dg/d\epsilon_p}\\
&= \frac{1}{E}[\sigma_{,\epsilon}(\epsilon_0) - \sigma(\epsilon_0)] > 0,
\end{aligned} \tag{A.7}$$

which is satisfied for strains prior to the ones corresponding to maximum load.

References

Brush, D., Almroth, B., 1975. Buckling of Bars, Plates, and Shells. McGraw-Hill I.

Budiansky, B., Hutchinson, J., 1964. Dynamic buckling of imperfection sensitive structures. In: Proceedings XI International Congress of Applied Mechanics, Munich.

Guduru, P., Freund, L., 2002. The dynamics of multiple neck formation and fragmentation in high rate extension of ductile materials. Int. J. Solids Struct. 39, 5615–5632.

Koning, C., Taub, J., 1933. Impact buckling of thin bars in the elastic range hinged at both ends. Luftfahrtfosrchung 10, 55–64.

Mainy, A., Ravi-Chandar, K. Dynamic buckling of thin metallic rings under external pressure, submitted for publication.

Mercier, S., Molinari, A., 2003. Predictions of bifurcation and instabilities during dynamic extension. Int. J. Solids Struct. 40, 1995–2016.

Nestorovic, M.D., Leroy, Y.M., Triantafyllidis, N., 2000. On the stability of rate-dependent solids with application to the uniaxial plane strain test. J. Mech. Phys. Sol. 48, 1467–1491.

Putelat, T., Triantafyllidis, N., 2014. Dynamic stability of externally pressurized elastic rings subjected to high rates of loading. Int. J. Solids Struct. 51, 1–12.

Shenoy, V., Freund, L., 1999. Necking bifurcations during high strain rate extension. J. Mech. Phys. Solids 47, 2209–2233.

Sorensen, N., Freund, L., 2000. Unstable neck formation in a ductile ring subjected to impulsive radial loading. Int. J. Solids Struct. 37, 2265–2283.

Xue, Z., Vaziri, A., Hutchinson, J., 2008. Material aspects of dynamic neck retardation. J. Mech. Phys. Solids 56, 93–113.

Zhang, H., Ravi-Chandar, K., 2006. On the dynamics of necking and fragmentation – I. Real-time and post-mortem observations in al 6061-O. Int. J. Fract. 142, 183–217.

Zhang, H., Ravi-Chandar, K., 2008. On the dynamics of necking and fragmentation—II. Effect of material properties, geometrical constraints and absolute size. Int. J. Fract. 150, 3–36.

Zhou, F., Molinari, J., Ramesh, K.T., 2006. An elastic–visco-plastic analysis of ductile expanding ring. Int. J. Impact Eng. 33, 880–891.